Simulating and detecting the quantum spin Hall effect in the kagome optical lattice

Guocai Liu,[1] Shi-Liang Zhu,[2] Shaojian Jiang,[1] Fadi Sun,[1] and W. M. Liu[1]

[1]*Beijing National Laboratory for Condensed Matter Physics, Institute of Physics, Chinese Academy of Sciences, Beijing 100190, China*

[2]*Laboratory of Quantum Information Technology, School of Physics and Telecommunication Engineering, South China Normal University, Guangzhou, China*

(Received 27 July 2010; published 4 November 2010)

We propose a model which includes a nearest-neighbor intrinsic spin-orbit coupling and a trimerized Hamiltonian in the kagome lattice and promises to host the transition from the quantum spin Hall insulator to the normal insulator. In addition, we design an experimental scheme to simulate and detect this transition in the ultracold atom system. The lattice intrinsic spin-orbit coupling is generated via the laser-induced-gauge-field method. Furthermore, we establish the connection between the spin Chern number and the spin-atomic density which enables us to detect the quantum spin Hall insulator directly by the standard density-profile technique used in atomic systems.

DOI: 10.1103/PhysRevA.82.053605 PACS number(s): 03.75.Hh, 05.30.Fk, 73.43.−f, 71.70.Ej

I. INTRODUCTION

The optical lattice system has gradually become a promising platform to simulate and study a lot of quantum phenomena in condensed-matter physics, because almost all parameters of the system can be well controlled [1]. Recent theoretical and experimental progress in laser-induced gauge field [2–7] makes it a hot spot to study topological quantum states [8] in cold atom system [9–15]. Subject to a compound's natural properties [16], the famous Haldane model [17] proposed two decades ago has not been confirmed by experiments, because the required periodic magnetic field cannot be easily implemented in actual material. For a topological insulator, an important extension from the Haldane model to a time-reversal invariant system [18–23], only a few materials are confirmed currently to have such exotic topological properties in nature [24–27], because the existence of such properties requires a relatively strong spin-orbit (SO) coupling. However, in an optical lattice system, we can engineer the lattice Hamiltonian to guarantee that this system hosts these novel topological phases [14]. Up to now, the neutral-cold-atom integer and fractional quantum Hall effects have been studied [28–30] and also the realization of the Haldane model has been designed by using the laser-induced-gauge-field method in an optical lattice [12].

In this paper, we propose a scheme to simulate and detect the two-dimensional (2D) quantum spin Hall (QSH) insulator in a kagome optical lattice with a trimer and a nearest-neighbor SO coupling term. With the laser-induced-gauge-field method, one can design a variety of lattice SO couplings [5,31–33], which is convenient for studying the 2D topological insulator in the optical lattice [9–11]. However, the original proposal [18] of realizing a 2D QSH insulator in a honeycomb lattice requires the next-nearest-neighbor hopping amplitude. This requirement makes it difficult to perform experiments in the optical lattice, because the high barrier makes the next-nearest-neighbor tunneling very small. Recently, a model [34] raised in a kagome lattice also requires the next-nearest-neighbor hopping. Interestingly, there is another QSH insulator model in the complicated kagome lattice. The inspiration comes from the fact that spin chirality in a ferromagnetic kagome lattice exerts important effects on the orbital magnetic moment and the anomalous quantum Hall effect [35]. We find that a kagome optical lattice with the trimer and SO coupling terms can host the 2D QSH insulator phase with only the nearest-neighbor hopping. Since the model only involves the nearest-neighbor hopping, it should be easier to implement in cold atomic experiments.

Furthermore, compared to condensed-matter systems, we find that detecting a QSH insulator has more advantages in an optical lattice system. Due to the time-reversal symmetry, the Chern number cannot be taken as a topological invariant to characterize the QSH insulator in a real electron system [36]. Chern number $C_\uparrow = +1$ ($C_\downarrow = -1$) in a QSH phase for the up-spin (down-spin) electrons, and the total Chern number $C = C_\uparrow + C_\downarrow = 0$. Since one cannot distinguish the contributions of conductance from up- or down-spin electrons with current technology, it is impossible to determine whether the system is in the QSH phase or normal phase by measuring Hall conductance. However, in cold atomic systems, it is the atom's internal state that represents the spin, not the real spin, which brings certain benefits to measurement. One can directly measure the spin Chern number to determine whether the system lies in the QSH phase, because optically measuring the atomic internal states is very simple. In this paper, we demonstrate that the method developed to detect the Chern number in cold atomic systems [12,30] can be put forward further to measure the spin Chern number, and thus we establish the connection between the spin Chern number and the spin-atomic density which enables us to detect the topological Chern numbers directly by the standard density-profile technique used in atomic systems.

The paper is organized as follows: In Sec. II, we introduce the model in a kagome lattice with both trimer and spin-orbital coupling. This model can realize the QSH phase with only the nearest-neighbor hopping terms; in Sec. III, we explain how to simulate this model in a cold-atom optical lattice, which includes designing the lattice SO coupling by using the laser-induced-gauge-field method; we present the method to detect the QSH phase in Sec. IV and give a brief summary in Sec. V.

II. MODEL

Let us consider the tight-binding model for two-component fermionic atoms on the kagome optical lattice, which consists

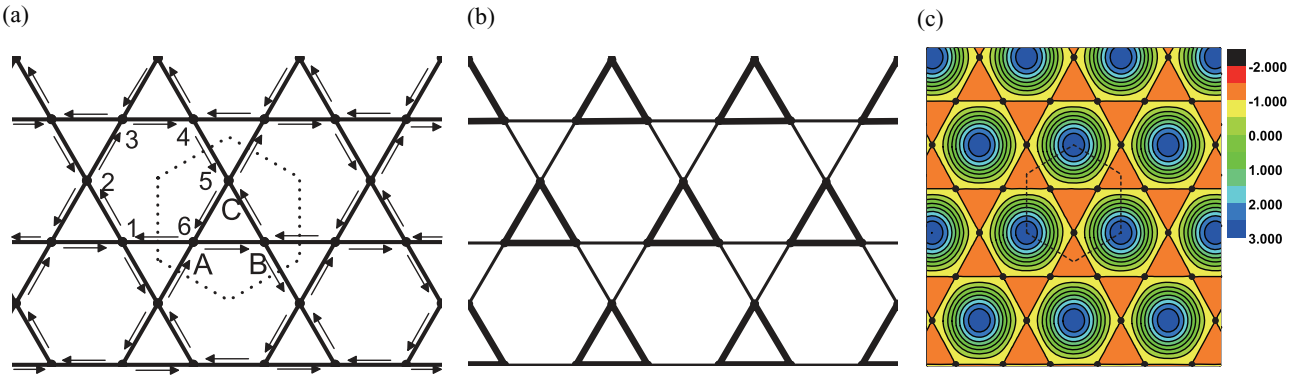

FIG. 1. (Color online) (a) Schematic of the nearest-neighbor intrinsic SO coupling in 2D kagome lattice. The up-spin atoms hop along (against) the arrowed direction with amplitude $i\lambda_{\rm SO}$ ($-i\lambda_{\rm SO}$). For the down-spin atoms, the arrows are reversed. The dashed line represents the Wigner-Seitz unit cell, which contains three independent sites (A, B, C). (b) The trimer kagome lattice. Hopping amplitude corresponds to $t+\kappa$ ($t-\kappa$) for the thick (thin) bonds. (c) Contours of the effective magnetic field for up-spin atoms defined by Eq. (21).

of three triangular sublattices A, B, and C (Fig. 1). The spin-independent part of the Hamiltonian is given by

$$H_0 = t_0 \sum_{mn\alpha} (b^\dagger_{m,n,\alpha} a_{m,n,\alpha} + b^\dagger_{m-1,n,\alpha} a_{m,n,\alpha} + c^\dagger_{m,n,\alpha} b_{m,n,\alpha} + c^\dagger_{m+1,n-1,\alpha} b_{m,n,\alpha} + a^\dagger_{m,n,\alpha} c_{m,n,\alpha} + a^\dagger_{m,n+1,\alpha} c_{m,n,\alpha}) + \text{H.c.}, \quad (1)$$

where t_0 is the hopping amplitude between the nearest-neighbor link, (m,n) labels the kagome unit cells with the unit vectors $\mathbf{b}_1 = (2,0)a$ and $\mathbf{b}_2 = (1,\sqrt{3})a$, $a^\dagger_{m,n,\alpha}$ ($a_{m,n,\alpha}$) is the creation (annihilation) operator of an atom with spin α (up or down) on lattice site (m,n) on sublattice A (an equivalent definition is used for sublattices B and C). For simplicity, we choose $t_0 = 1$ as the energy unit and the distance between the nearest sites a as the length unit throughout this paper.

By using the Fourier transform of atomic operators $a_{m,n,\alpha}$, i.e.,

$$a_{m,n,\alpha} = \frac{1}{\sqrt{N}} \sum_{\mathbf{k}} a_{\mathbf{k}\alpha} e^{-i\mathbf{k}\cdot\mathbf{R}^A_{mn}}, \quad (2)$$

the Hamiltonian (1) can be diagonalized in the momentum space as

$$H_0 = \sum_{\mathbf{k}} \psi^+_{\mathbf{k}} [\mathcal{H}_0(\mathbf{k}) \otimes \mathbf{I}_{2\times 2}] \psi_{\mathbf{k}}, \quad (3)$$

where $\mathbf{I}_{2\times 2}$ is a 2×2 unit matrix. The six-component basis operator $\psi_{\mathbf{k}} = (a_{\mathbf{k}\uparrow}, b_{\mathbf{k}\uparrow}, c_{\mathbf{k}\uparrow}, a_{\mathbf{k}\downarrow}, b_{\mathbf{k}\downarrow}, c_{\mathbf{k}\downarrow})^{\rm T}$ describes an atom in the corners of the kagome lattice unit cell (Fig. 1) with spin α ($\uparrow$ and $\downarrow$). Here $\mathcal{H}_0(\mathbf{k})$ is a 3×3 spinless matrix given by

$$\mathcal{H}_0(\mathbf{k}) = \begin{pmatrix} 0 & 2\cos P_1 & 2\cos P_3 \\ 2\cos P_1 & 0 & 2\cos P_2 \\ 2\cos P_3 & 2\cos P_2 & 0 \end{pmatrix}, \quad (4)$$

where we have defined $P_1 = \mathbf{k}\cdot\mathbf{a}_1$, $P_2 = \mathbf{k}\cdot\mathbf{a}_2$, and $P_3 = \mathbf{k}\cdot\mathbf{a}_3$, with $\mathbf{a}_1 = (1,0)$, $\mathbf{a}_2 = (-1/2, \sqrt{3}/2)$, and $\mathbf{a}_3 = (-1/2, -\sqrt{3}/2)$ representing the displacements in a unit cell from A to B site, from B to C site, and from C to A site, respectively. In this notation, the first Brillouin zone is a hexagon with the corners of $\mathbf{K} = \pm(2\pi/3)\mathbf{a}_1$, $\pm(2\pi/3)\mathbf{a}_2$, $\pm(2\pi/3)\mathbf{a}_3$, and two of which are independent.

The energy spectrum for spinless Hamiltonian $\mathcal{H}_0(\mathbf{k})$ is characterized by one dispersionless flat band ($\epsilon^{(0)}_{1\mathbf{k}} = -2$), which reflects the fact that the 2D kagome lattice is a line graph of the honeycomb structure [37], and two dispersive bands, $\epsilon^{(0)}_{2(3)\mathbf{k}} = 1 \mp \sqrt{4b_{\mathbf{k}} - 3}$ with $b_{\mathbf{k}} = \sum_{i=1}^{3} \cos^2(\mathbf{k}\cdot\mathbf{a}_i)$. These two dispersive bands touch at Dirac points $\mathbf{K}$ and exhibit a cusp, $\epsilon^{(0)}_{2(3)\mathbf{k}} = (1 \mp \sqrt{3}|\mathbf{k}-\mathbf{K}|)$.

When the following intrinsic SO coupling term is taken into account in the kagome lattice model, as illustrated in Fig. 1(a), the gap will be opened at the two inequivalent Dirac points. The tight-binding expression for this SO coupling Hamiltonian can be given as follows:

$$H_{\rm SO} = i\lambda_{\rm SO} \sum_{m,n} (b^\dagger_{m,n}\sigma_z a_{m,n} + b^\dagger_{m-1,n}\sigma_z a_{m,n} + c^\dagger_{m,n}\sigma_z b_{m,n} + c^\dagger_{m+1,n-1}\sigma_z b_{m,n} + a^\dagger_{m,n}\sigma_z c_{m,n} + a^\dagger_{m,n+1}\sigma_z c_{m,n}) + \text{H.c.}, \quad (5)$$

where $\lambda_{\rm SO}$ is the SO coupling constant, σ_z is the Pauli matrix, and $a^\dagger_{m,n} = (a^\dagger_{m,n,\uparrow}, a^\dagger_{m,n,\downarrow})$. Taking the Fourier transform (2) and considering the $\psi_{\mathbf{k}}$ below Eq. (3), we have $H_{\rm SO} = \sum_{\mathbf{k}} \psi^+_{\mathbf{k}} \mathcal{H}_{\rm SO}(\mathbf{k}) \psi_{\mathbf{k}}$, where

$$\mathcal{H}_{\rm SO}(\mathbf{k}) = \begin{pmatrix} \mathcal{H}_+(\mathbf{k}) & 0 \\ 0 & \mathcal{H}_-(\mathbf{k}) \end{pmatrix}, \quad (6)$$

with

$$\mathcal{H}_\pm(\mathbf{k}) = \pm 2i\lambda_{\rm SO} \begin{pmatrix} 0 & -\cos P_1 & \cos P_3 \\ \cos P_1 & 0 & -\cos P_2 \\ -\cos P_3 & \cos P_2 & 0 \end{pmatrix}. \quad (7)$$

This SO coupling destroys spin SU(2) symmetry and opens a band gap $\Delta_{\rm SO} = \sqrt{3}\lambda_{\rm SO}$ at the Dirac point.

Lattice trimerization can break the inversion symmetry of the kagome lattice and also open a gap at the Dirac point [34].

It is described by

$$H_{\rm trim} = \sum_{mn\alpha}[\kappa(b^{\dagger}_{m,n,\alpha}a_{m,n,\alpha} - b^{\dagger}_{m-1,n,\alpha}a_{m,n,\alpha}) + \kappa(c^{\dagger}_{m,n,\alpha}b_{m,n,\alpha} - c^{\dagger}_{m+1,n-1,\alpha}b_{m,n,\alpha}) + \kappa(a^{\dagger}_{m,n,\alpha}c_{m,n,\alpha} - a^{\dagger}_{m,n+1,\alpha}c_{m,n,\alpha})] + \text{H.c.}, \quad (8)$$

where κ describe an alternating pattern of bond hopping integrals along the three principal spatial directions as illustrated in Fig. 1(b). Taking the Fourier transform (2) again, the trimerized Hamiltonian can be rewritten as $H_{\rm trim} = \sum_{\mathbf{k}} \psi^{+}_{\mathbf{k}}[\mathcal{H}_{\rm trim}(\mathbf{k}) \otimes \mathbf{I}_{2\times 2}]\psi_{\mathbf{k}}$ with

$$\mathcal{H}_{\rm trim}(\mathbf{k}) = 2i \begin{pmatrix} 0 & -\kappa \sin P_1 & \kappa \sin P_3 \\ \kappa \sin P_1 & 0 & -\kappa \sin P_2 \\ -\kappa \sin P_3 & \kappa \sin P_2 & 0 \end{pmatrix} \quad (9)$$

for both spin components.

We take the above SO coupling and trimerized Hamiltonian as perturbation, which means $\lambda_{\rm SO} \ll t$ and $\kappa \ll t$. Although both of perturbations can bring gaps at Dirac points independently, these two gaps have different topological natures. As we will show in the following, the former is nontrivial and the quantum spin Hall effect will occur if the Fermi energy level locates in the gap; the latter is a trivial gap.

In order to prove the above assertion, we expand the total Hamiltonian $\mathcal{H}(\mathbf{k}) = \mathcal{H}_0(\mathbf{k}) + \mathcal{H}_{\rm SO}(\mathbf{k}) + \mathcal{H}_{\rm trim}(\mathbf{k})$ at two inequivalent points $\mathbf{K}_{\pm} = (\pm\frac{2\pi}{3},0)$, then take $\mathbf{k}\cdot\mathbf{p}$ perturbation theory to get its effective Hamiltonian. At last, projecting it onto band 2 and 3 subspaces, we get four independent Dirac Hamiltonians,

$$\mathcal{H}^{K}_{s\sigma} = -s\upsilon_F k_x \tau_z + s\upsilon_F k_y \tau_x + m_{s\sigma}\tau_y, \quad (10)$$

where $s = \pm 1$ and $\sigma = \pm 1$ represent different valleys $\mathbf{K}_{\pm}$ and spin indices, respectively, $\upsilon_F = \sqrt{3}t$ is Fermi velocity, and τ_i are Pauli matrices with $i = x,y,z$. The Dirac mass $m_{s\sigma} = \sqrt{3}\sigma\lambda_{\rm SO} - 3s\kappa$.

We now address the topological properties of this model. The system is in the QSH phase when the SO coupling dominates in the condition $|\lambda_{\rm SO}| > |\sqrt{3}\kappa|$; otherwise, the system is in the normal phase. It can be proved by directly calculating the Z_2 topological invariant [18,20]. Alternatively, one can also understand the topological phases from the view of the spin Chern number [36]. In order to do that, we apply a uniform magnetic field along the z direction with gauge vector $\mathbf{A}(\mathbf{r}) = (0,\mathcal{B}x,0)$ and obtain the Landau energy levels

$$E^{s\sigma}_{n} = \begin{cases} m_{s\sigma}\,\mathrm{sgn}\,(e\mathcal{B}) & n = 0 \\ \pm\sqrt{2n\hbar\upsilon_F^2|e\mathcal{B}| + m^2_{s\sigma}} & n = 1,2,3,\ldots \end{cases} \quad (11)$$

By using the Green's function theory [12], we can get the Chern number

$$C_{s\sigma} = \tfrac{1}{2}\mathrm{sgn}\big(E^{s\sigma}_0\big) = \tfrac{1}{2}\mathrm{sgn}[m_{s\sigma}\,\mathrm{sgn}\,(e\mathcal{B})] \quad (12)$$

between the energy interval $-|m_{s\sigma}| < \mu < |m_{s\sigma}|$ with μ being the Fermi energy (Fig. 2). Actually it is the sign of $n = 0$ energy (zero-mode) which determines the Chern number. As an example, we focus on $\mu = 0$ and take $e\mathcal{B} > 0$ throughout this paper to see the difference more clearly between the QSH phase and the normal phase. For the QSH phase, we take $\lambda_{\rm SO} > \sqrt{3}\kappa > 0$, and it is easy to see that for up-spin atoms, $m_{s=\pm1,\uparrow} > 0$ and then $C_{\uparrow} = C_{+1,\uparrow} + C_{-1,\uparrow} = 1$. For down-spin atoms, $m_{s=\pm1,\downarrow} < 0$ and $C_{\downarrow} = C_{+1,\downarrow} + C_{-1,\downarrow} = -1$. However, if we take $\sqrt{3}\kappa > \lambda_{\rm SO} > 0$, which corresponds to the normal phase, $C_{\uparrow} = C_{\downarrow} = 0$ for both up- and down-spin atoms. In the QSH phase, the Chern numbers with different spin components have the same value but with opposite sign. Whereas if it is in normal phase, the Chern numbers equal zero for both up- and down-spin atoms.

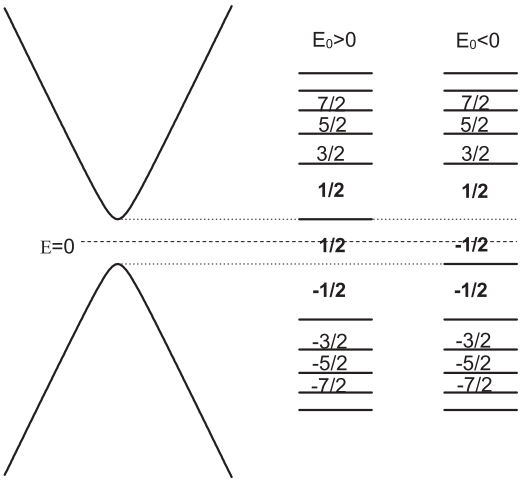

FIG. 2. Effect on Chern number by the sign of $n = 0$ Landau energy level. The left figure corresponds to disperse relation of Eq. (10) without the magnetic field. The right two columns show the Chern numbers when the magnetic field is applied and Fermi energy is located at different intervals for two cases with $E_0 > 0$ and $E_0 < 0$. Here E_0 denotes the $n = 0$ Landau energy level. The dashed line represents zero energy, and the dotted lines give the original band gap.

To further understand the topological properties of the model, we show the edge state effects in Fig. 3. From Fig. 3(a), we can see that there is a pair of chiral gapless edge states for every band gap when the SO coupling dominates. This means that the system is in topological insulator phases at 1/3 and 2/3 filling. When only a trimer term exists, it opens a band gap at the Dirac point, but no edge states connect the upper and lower bands [see Fig. 3(b)], therefore the system is in normal insulator phase at 2/3 filling. On the other hand, we also see that the trimer term cannot open a gap between bands 1 and 2 [Fig. 3(b)]. Therefore the system at 1/3 filling will be still in the topological insulator phase when two perturbations are present but the trimer term dominates [see Fig. 3(c)].

III. SIMULATION

In this section we introduce an approach to simulate the kagome lattice with the trimer and SO coupling terms in an optical lattice system. To this end, two problems need to be solved. One is how to generate the kagome optical lattice with the trimer terms; the other is how to simulate the lattice SO coupling. For the first problem, we use the superlattice technique addressed in Refs. [38–40], that is, three superlaser beams with the same wave-vector length but different polarizations are applied along three different

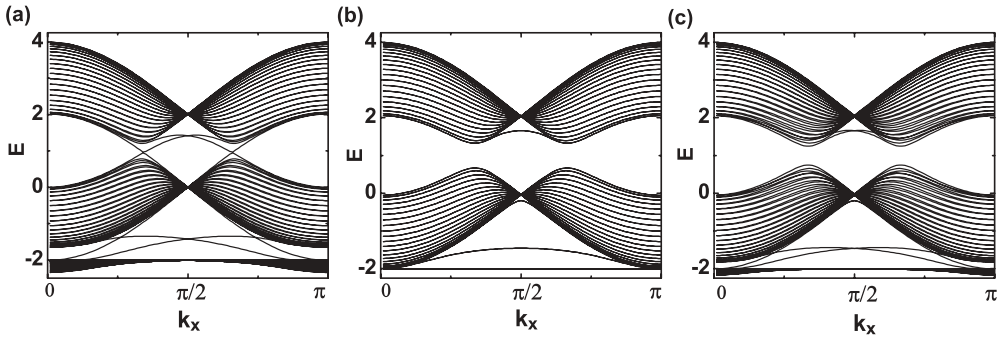

FIG. 3. The band structure of the lattice model in the striped geometry. We take $\lambda_{SO} = 0.1$, $\kappa = 0$ for (a), $\lambda_{SO} = 0$, $\kappa = 0.1$ for (b), and $\lambda_{SO} = 0.05$, $\kappa = 0.1$ for (c).

directions: $\mathbf{e}_y$ and $\frac{1}{2}\mathbf{e}_y \pm \frac{\sqrt{3}}{2}\mathbf{e}_x$, respectively. In our proposal, each superlaser beam consists of four large detuned standing-wave lasers with the same polarization but different wave-vector lengths in the x-y plane. The total potential is thus given by

$$V(\mathbf{r}) = V_0 \sum_{i=1}^{3} \{\cos(\mathbf{k}_i \cdot \mathbf{r} + 3\delta_i\varphi/2) + 2\cos(\mathbf{k}_i \cdot \mathbf{r}/3 + \delta_i\varphi/2) + 4\cos(\mathbf{k}_i \cdot \mathbf{r}/9 + \delta_i\varphi/6) + \zeta \cos[\mathbf{k}_i \cdot \mathbf{r}/9 + \delta_i(\varphi/6 + \pi/2)]\}^2, \quad (13)$$

with the wave vectors $\mathbf{k}_1 = (\frac{\sqrt{3}}{2}, \frac{1}{2})k$, $\mathbf{k}_2 = (-\frac{\sqrt{3}}{2}, \frac{1}{2})k$, $\mathbf{k}_3 = (0,1)k$, and $\delta_1 = \delta_2 = -\delta_3 = 1$. First, we consider the case with $\zeta = 0$. One can get a triangular lattice when $\varphi = 0$ or 2π and a kagome lattice when $0 < \varphi < 2\pi$. A uniform kagome lattice corresponds to $\varphi = \pi$, as shown in Fig. 4(a). When φ takes other values, one can obtain the trimerized kagome lattice accompanying distortion of the lattice structure [38–40]. When we increase the strength of the trimerized Hamiltonian, the kagome lattice will be distorted. To overcome this defect, we add another laser beam which corresponds to the $\zeta \neq 0$ in Eq. (13) and assume $\varphi = \pi$ all the time. The added laser will interfere with primary lasers and generate the trimerized kagome lattice. ζ is an adjustable parameter to control the strength of trimerized Hamiltonian. With this method, the kagome lattice will not have an obvious offset from the uniform one even if ζ takes a relatively large value. As shown in Fig. 4(b), the parameter $\zeta = 1.5$ is chosen as a typical example.

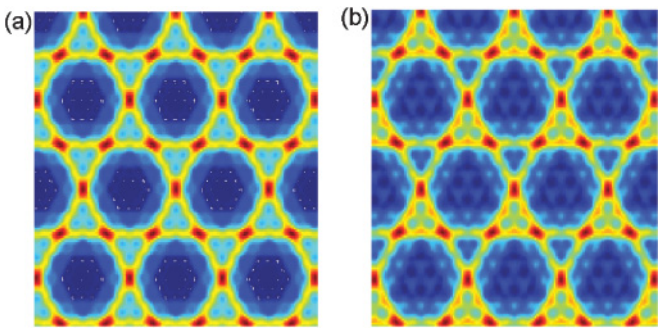

FIG. 4. (Color online) (a) A uniform kagome lattice for $\varphi = \pi$ and $\zeta = 0$. (b) A trimer kagome lattice for $\varphi = \pi$ and $\zeta = 1.5$.

We now focus on how to simulate the lattice SO coupling. Using the laser-induced-gauge-field method, it has been proposed that both Abelian and non-Abelian gauge fields can be simulated in cold atomic systems. In addition, experiments to achieve such artificial gauge fields have been reported [6,7]. Interestingly, it has been proposed that a periodic magnetic field, which is not easy to be realized in a condensed-matter system, can be created by two opposite-traveling standing-wave laser beams [5]. In the following, we will show in an explicit manner that the artificial gauge field proposed in Ref. [5] is equivalent to a SO coupling. Furthermore, the required lattice SO coupling addressed in the previous section can also be achieved in a suitable configuration of the laser beams.

In optical lattice systems, cold atoms can hop between adjacent sites. According to Peierls theory, the additional gauge vector potential $\mathbf{A}$ makes the hopping obtain a phase factor $\exp(i\frac{e}{\hbar}\int \mathbf{A} \cdot \mathbf{dl})$, where the integral is along the hopping path. If the atom has multiple states, which correspond to different spin components, vector potential $\mathbf{A}$ should be a matrix. After taking such an approximation, that is, $t_{ij}^{\alpha\beta} = t_{ij}$, where α, β indicate any spin index, the correction to atom hopping between different sites coming from the gauge field is equivalent to a unitary operator [41]. For a two-component atom system, the unitary operator can be written as

$$U_{ij} = e^{i\alpha_{ij}\sigma_{ij}} = \cos\alpha_{ij} + i\sigma_{ij}\sin\alpha_{ij}, \quad (14)$$

where i, j represent different site indices, and α_{ij} is the gauge flux and depends on the hopping integral. Here σ_{ij} is the Pauli matrix, whose specific form depends on the gauge vector potential. Therefore, a tight-binding Hamiltonian of atoms can be written as

$$\bar{H} = \sum_{\langle i,j\rangle} (t_{ij}\bar{a}_j^\dagger U_{ij}\bar{a}_i + \text{H.c.}) = \bar{H}_0 + \bar{H}_{SO}, \quad (15)$$

with

$$\bar{H}_0 = \sum_{\langle i,j\rangle} (t_{ij}\cos\alpha_{ij})\bar{a}_j^\dagger\bar{a}_i + \text{H.c.}, \quad (16)$$

$$\bar{H}_{SO} = i\sum_{\langle i,j\rangle} (t_{ij}\sin\alpha_{ij})\bar{a}_j^\dagger\sigma_{ij}\bar{a}_i + \text{H.c.} \quad (17)$$

Here $\langle i,j\rangle$ denotes the nearest-neighbor hopping, and $\bar{a}_i$ ($\bar{a}_i^\dagger$) the creation (annihilation) operator on site i. The first term is the normal Hamiltonian, while the second one is equivalent to

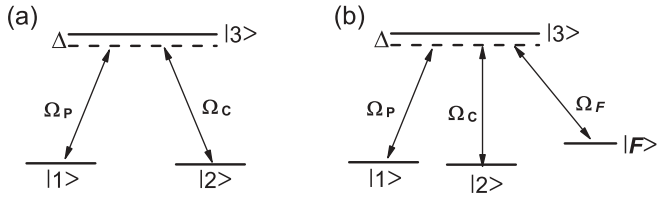

FIG. 5. (a) Three-level Λ-type atoms coupling with two laser beams with Rabi frequencies Ω_p and Ω_c. (b) A different hyperfine level $|F\rangle$ for detection which can be coupled to the excited state $|3\rangle$ by Rabi frequency Ω_F.

SO coupling. From the above equations, we can observe the following: (i) By choosing suitable Pauli matrix σ_{ij}, one can simulate various SO couplings existing in actual materials. For our model, we should choose $\sigma_{ij} = \sigma_z$. (ii) Through adjusting the gauge flux α_{ij}, one can change the relative strength between the two terms. For example, $\alpha_{ij} = 0$ corresponds to no SO coupling, while $\alpha_{ij} = \pi/2$ is equivalent to only the SO coupling interaction existing in the system. This facilitates us to study the nature brought by SO coupling.

We now address the approach to achieve the intrinsic SO coupling described in Eq. (5). To this end, we consider a cold atomic system with each atom having a Λ-type level configuration [Fig. 5(a)]. The ground states $|1\rangle$ and $|2\rangle$ are coupled to the excited state $|3\rangle$ through a spatially varying standing-wave laser field, with Rabi frequencies $\Omega_p = \Omega \sin\theta e^{-iS_1}$ and $\Omega_c = \Omega \cos\theta e^{-iS_2}$, respectively. With the rotating-wave approximation, the laser-atom coupling Hamiltonian is given by

$$\hat{H}_{\rm int} = -\frac{\hbar}{2}\begin{pmatrix} 0 & 0 & \Omega_p \\ 0 & 0 & \Omega_c \\ \Omega_p^* & \Omega_c^* & -2\Delta \end{pmatrix}, \tag{18}$$

with the eigenstates (the dressing states)

$$\begin{aligned} |\chi_1\rangle &= e^{-iS_1}\cos\theta|1\rangle - e^{-iS_2}\sin\theta|2\rangle, \\ |\chi_2\rangle &= \cos\varphi\sin\theta e^{-iS_1}|1\rangle + \cos\varphi\cos\theta e^{-iS_2}|2\rangle - \sin\varphi|3\rangle, \\ |\chi_3\rangle &= \sin\varphi\sin\theta e^{-iS_1}|1\rangle + \sin\varphi\cos\theta e^{-iS_2}|2\rangle + \cos\varphi|3\rangle, \end{aligned}$$

and eigenvalues $\lambda_{n=1,2,3} = 0, \frac{\hbar}{2}(\Delta \mp \sqrt{\Delta^2+\Omega^2})$. Here, single-photon detuning $\Delta = \omega_3 - \omega_1 - \omega_p$, with ω_3, ω_1, ω_p the intrinsic frequency of atom states $|3\rangle$, $|1\rangle$ and laser Ω_p, respectively. In the new basis space $|\chi\rangle = \{|\chi_1\rangle, |\chi_2\rangle, |\chi_3\rangle\}$, the primary atom Hamiltonian $\hat{H} = \frac{\mathbf{p}^2}{2M} + \hat{H}_{\rm int}(\mathbf{r}) + \hat{V}(\mathbf{r})$ can be rewritten as $H = \frac{1}{2M}(-i\hbar\nabla - \mathbf{A})^2 + V$ with M the atom mass, $\mathbf{A}$ and V being matrix with matrix element $\mathbf{A}_{n,m} = i\hbar\langle\chi_n(\mathbf{r})|\nabla\chi_m(\mathbf{r})\rangle$, and $V_{n,m} = \lambda_n(\mathbf{r})\delta_{n,m} + \langle\chi_n(\mathbf{r})|\hat{V}(\mathbf{r})|\chi_m(\mathbf{r})\rangle$, respectively. One can see that in the new basis the atom can be considered as moving in the gauge potential $\mathbf{A}$, which corresponds to an effective magnetic field $\mathbf{B}_{\rm eff} = (\nabla \times \mathbf{A}) - \frac{i}{\hbar}(\mathbf{A} \times \mathbf{A})$ [2,12].

We focus on the subspace spanned by the two lower eigenstates $\{|\chi_1\rangle, |\chi_2\rangle\}$, which is redefined by $|\chi_\uparrow\rangle \equiv |\chi_1\rangle$ and $|\chi_\downarrow\rangle \equiv |\chi_2\rangle$ with the spin language. This gives an effective spin-1/2 system. For the large detuning ($\Delta \gg \Omega$) case, both states $|\chi_\uparrow\rangle$ and $|\chi_\downarrow\rangle$ are stable under atomic spontaneous emission from the initial excited state $|3\rangle$. Furthermore, we assume the adiabatic condition, which requires the off-diagonal elements of the matrices $\mathbf{A}$ are smaller than the eigenenergy differences $|\lambda_m - \lambda_n|$ $(m, n = 1,2,3)$ of the states $|\chi_m\rangle$. Under this adiabatic condition and in the basis space $\{|\chi_\uparrow\rangle, |\chi_\downarrow\rangle\}$, the gauge potential $\mathbf{A}$ becomes diagonal and takes the form [5]

$$\mathbf{A} = \begin{pmatrix} \mathbf{A}_\uparrow & 0 \\ 0 & \mathbf{A}_\downarrow \end{pmatrix}, \tag{19}$$

with

$$\mathbf{A}_\uparrow = -\mathbf{A}_\downarrow = \hbar(\nabla S_1 \cos^2\theta + \nabla S_2 \sin^2\theta).$$

Here we neglect the correction to nearest-neighbor tunneling brought by the change of potential $V(\mathbf{r})$ because of the large detuning approximation.

We consider a specific configuration of the laser beams with two opposite-traveling standing-wave laser beams [5,12], which take the Rabi frequencies $\Omega_p = \Omega\sin(k_2 y + \frac{\pi}{4})e^{i(k_1 x + k_z z)}$ and $\Omega_c = \Omega\cos(k_2 y + \frac{\pi}{4})e^{-i(k_1 x + k_z z)}$. The effective gauge potential is generated as $\mathbf{A}_\uparrow = -\mathbf{A}_\downarrow = \hbar\sin(2k_2 y + 2\phi_1)(k_1\mathbf{e}_x + k_z\mathbf{e}_z)$. Here $k_1 = k\sin\theta_1\cos\theta_2$, $k_2 = k\cos\theta_1$, and $k_z = k\sin\theta_1\sin\theta_2$ with k the wave-vector number of the laser, θ_1 the angle between the wave vector and the $\mathbf{e}_y$ axis, θ_2 the angle between the $\mathbf{e}_x$ axis and the plane consisting of the wave vector and $\mathbf{e}_y$ axis. We emphasize that the choice of wave vector k_2 of the laser beams must be a multiple of $\pi/\sqrt{3}$ in order to be commensurate with the optical lattice. We take $k_2 = \pi/\sqrt{3}$. The Peierls phase factors for the nearest-neighbor hopping in Fig. 1(a) are $\varphi_{12}^\alpha = \varphi_{23}^\alpha = \varphi_{45}^\alpha = \varphi_{56}^\alpha = -\alpha\frac{\sqrt{3}k_1}{3k_2} = -\alpha\frac{k_1}{\pi}$ and $\varphi_{34}^\alpha = \varphi_{61}^\alpha = 0$ with $\alpha = \pm 1$ representing the up and down spins. Considering the symmetry of the kagome lattice, the vector potential $\mathbf{A}$ is rotated by $\pm 2\pi/3$ to obtain the other two vector potentials. Therefore, the total effective vector potential and magnetic field can be written as

$$\begin{aligned} \mathbf{A}_{\rm eff}^\alpha = \alpha\hbar k_1\{&[\sin(2k_2 y) - \cos(k_2 y)\sin(\sqrt{3}k_2 x)]\mathbf{e}_x \\ &+ \sqrt{3}\sin(k_2 y)\cos(\sqrt{3}k_2 x)\mathbf{e}_y\}, \end{aligned} \tag{20}$$

$$\mathbf{B}_{\rm eff}^\alpha = -\alpha\frac{2\pi\hbar k_1}{\sqrt{3}}[2\sin(k_2 y)\sin(\pi x) + \cos(2k_2 y)]\mathbf{e}_z. \tag{21}$$

It should be noticed that we have dropped the $\mathbf{e}_z$ component in Eq. (20) because the integral for Peierls phase is only in the x-y plane. The contours of the magnetic field for up spin are plotted in Fig. 1(c). However, the total accumulated phases for the nearest-neighbor hopping along the arrowed directions in Fig. 1(a) are

$$\begin{aligned} \varphi_{61}^\alpha = \varphi_{45}^\alpha = \varphi_{34}^\alpha = \varphi_{12}^\alpha = \varphi_{23}^\alpha = \varphi_{56}^\alpha \\ = -\alpha\frac{2k\sin\theta_1\cos\theta_2}{\pi} = \alpha\varphi. \end{aligned} \tag{22}$$

We must retain θ_1 to satisfy $k_2 = \pi/\sqrt{3}$. However, we can alter φ, which controls the relative strength between the SO coupling and the ordinary hopping terms, by changing the angle θ_2 in the x-z plane. So, we can replace $t_{ij}\cos\alpha_{ij} \to t\cos\varphi$ in Eq. (16) and $t_{ij}\sin\alpha_{ij} \to t\sin\varphi \to \lambda_{\rm SO}$ in Eq. (17) and therefore get the intrinsic SO coupling model in our cold-atomic kagome optical lattice.

IV. DETECTION

For the quantum Hall effect in a two-dimensional electronic gas in a condensed-matter system, Hall conductivity σ_{xy} and Chern number satisfy the relation $\sigma_{xy}=\frac{e^2}{h}C$ with h the Planck constant and e electronic charge. Thus one can usually detect the Chern number through measuring Hall conductivity. However, the detection of the spin Chern number in actual material systems is a challenge, because one cannot distinguish the contributions of the conductivity from up- and down-spin electrons.

Compared to an electronic system, we will show that a significant advantage of an atomic system is that the spin Chern number can be directly verified by using a method similar to the method used to detect the (mass) Chern number. It has been shown that the conductivity σ_{xy} (Chern number) is related to the atomic density from the Streda formula $\sigma_{xy} = \partial\rho/\partial\mathcal{B}|_{\mu,T}$ when a uniform magnetic field $\mathcal{B}$ is applied in the system. Thus one can measure the Chern number through the detection of the density profile, which is a standard detection method used in an atomic system [12,30]. Since the internal state-dependent image has also been achieved, the similar method can be straightforward expanded to measure the spin Chern number. Therefore we may establish the relation between the spin Chern and atom density, enabling us to detect the QSH phase of the system via the density-profile measurement technique.

We now introduce how to detect the QSH phase in an ultracold-atomic optical lattice. In a cold atomic system, the information of quantum states is usually measured from the density-profile image. So we will first derive the spin-atomic density from the Dirac Hamiltonian (10), and then obtain the information of the Chern number of the system.

The uniform magnetic field can be simulated by rotating the optical lattice at a constant frequency $\omega = e\mathcal{B}/2M$. From the Landau energy levels obtained at Eq. (11), we get the density [12] for every Dirac Hamiltonian (10) as

$$\rho_{s\alpha} = \sum_{n=0}^{+\infty} \frac{\mathrm{sgn}(\mu)\mathcal{B}}{2\phi_0}[\Theta(|\mu|-E_{n+1})+\Theta(|\mu|-E_n)] + \frac{\mathcal{B}}{2\phi_0}\frac{m_{s\alpha}}{|m_{s\alpha}|}\Theta(|m_{s\alpha}|-|\mu|), \quad (23)$$

where Θ stands for the unit step function, μ is the chemical potential, and ϕ_0 the flux quantum. The second term of Eq. (23) is the atom density coming from $n = 0$ (zero-mode), similar to the discussion of the Chern number (see Fig. 2). The calculated spin-atomic density $\rho_\alpha = \rho_{+\alpha} + \rho_{-\alpha}$ ($\alpha =\uparrow,\downarrow$) in units of $\mathcal{B}/\phi_0$ is plotted as a function of the normalized chemical potential μ/m_0 (for $\hbar v_F^2|e\mathcal{B}| = 4|m_0|^2$) in Fig. 6. It is essential that the spatial density profile is uniquely determined by the function $\rho(\mu/m_0)$ in the local density approximation, which is typically well satisfied for trapped fermions. We focus on the point $\mu = 0$ where the Dirac mass makes its central effect on the density or Chern number. When the system is in the QSH phase, for example, we take the parameters $\sqrt{3}\lambda_{\mathrm{SO}} > 3\kappa > 0$, specially assuming $|m_{+\uparrow}| = |m_{-\downarrow}| = 0.5|m_{-\uparrow}| = 0.5|m_{+\downarrow}| = 0.5m_0$, then we have $m_{-\uparrow} > m_{+\uparrow} > 0 > m_{-\downarrow} > m_{+\downarrow}$. The spin-atomic density is shown in Figs. 6(a) and 6(b). It is easy to see that the up-spin-atomic density $\rho_\uparrow = \mathcal{B}/\phi_0 > 0$ [Fig. 6(a)] and the down one $\rho_\downarrow = -\mathcal{B}/\phi_0 < 0$ [Fig. 6(b)]. For the normal phase, we take $3\kappa > \sqrt{3}\lambda_{\mathrm{SO}} > 0$ and assume $|m_{+\uparrow}| = |m_{-\downarrow}| = 0.5|m_{-\uparrow}| = 0.5|m_{+\downarrow}| = 0.5m_0$, which means $m_{-\uparrow} > m_{+\uparrow} > 0 > m_{-\downarrow} > m_{+\downarrow}$. We obtain $\rho_{\uparrow,\downarrow} = 0$ [Figs. 6(c) and 6(d)]. The spin-atomic density shows a relation similar to that at the conclusion of spin Chern number theory. This is not surprising because according to the Streda formula and from Eq. (23), it is easy to obtain the relation between the spin Chern number and the spin-atomic density as

$$C_\alpha = \rho_\alpha\phi_0/\mathcal{B}. \quad (24)$$

This formula provides us the approach to measure whether the system is in the QSH phase. First, we measure the spin-atomic density and denote it as $\rho^0_{\uparrow,\downarrow}$ at $\mu = 0$ in the absence of $\mathcal{B}$. Then the optical lattice is rotated to generate the effective uniform magnetic field $\mathcal{B}$, and the new density of the cold atoms $\rho^1_{\uparrow,\downarrow}$ is measured again. If $\rho^1_\uparrow > \rho^0_\uparrow$ and $\rho^1_\downarrow < \rho^0_\downarrow$, the system is in the QSH insulator phase. However, if $\rho^1_{\uparrow,\downarrow} = \rho^0_{\uparrow,\downarrow}$, the system is in the normal insulator phase. Since the density difference is actually quantized in units of $\mathcal{B}/\phi_0$, the above method could be rather robust.

It is clear from Eq. (24) that the total Chern number $C = C_\uparrow + C_\downarrow = 0$, and thus the direct detection of the QSH phase is a challenge in an electronic system. However the QSH phase can be directly verified in atomic systems, since the densities $\rho_\uparrow$ and $\rho_\downarrow$ can be separately detected [5]. To experimentally detect the spin-atomic density, we need first transfer the dressed state $|\chi_\downarrow\rangle$ to a different hyperfine level $|F\rangle$ which is coupled to the excited state $|3\rangle$ by a laser pulse (with a Rabi frequency Ω_F), as seen in Fig. 5(b). This pulse, together with the original laser beams Ω_p and Ω_c, make a Raman transition with an effective Hamiltonian $H_R = (\Omega_F^*\Omega/\Delta)|\chi_\downarrow\rangle\langle F| + \mathrm{H.c.}$ (note that the state $|\chi_\uparrow\rangle$ is still decoupled because of the phase relation between Ω_p and

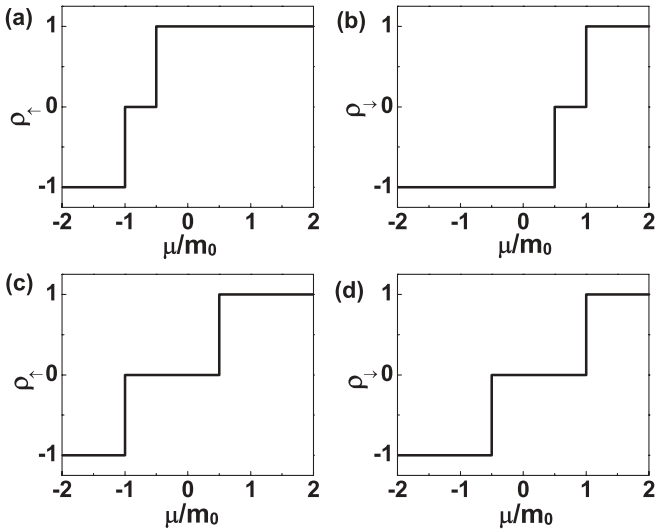

FIG. 6. The spin-atomic density in units $\mathcal{B}/\phi_0$ as a function of the normalized chemical potential μ/m_0 with the definition $\hbar v_F^2|e\mathcal{B}| = 4|m_0|^2$. (a) and (b) correspond to the QSH phase case with $\sqrt{3}\lambda_{\mathrm{SO}} > 3\kappa > 0$; (c) and (d) correspond to the normal phase case with $\sqrt{3}\lambda_{\mathrm{SO}} < 3\kappa < 0$. $\rho_\uparrow$ ($\rho_\downarrow$) denotes the up-(down-)spin-atomic density.

Ω_c) [5]. Although the form of the state $|\chi_\downarrow\rangle$ is spatially varying, the Rabi frequency Ω (and thus also $\Omega_F^*\Omega/\Delta$) is spatially constant. A complete Raman transition with a π pulse will transfer all of the atoms that are in the dressed state $|\chi_\downarrow\rangle$ to the hyperfine state $|F\rangle$. After this operation, the initial different dressed spin states are mapped to different hyperfine levels, and the populations in different atomic hyperfine levels can be separately imaged with the known experimental techniques.

V. SUMMARY

In summary, we have proposed a model which promises to host the transition from the QSH insulator phase to the normal insulator phase in the 2D kagome optical lattice. The model includes two kinds of periodic perturbations, i.e., a nearest-neighbor intrinsic SO coupling and a trimerized Hamiltonian. The competition between them determines the system's phase. Then we demonstrated that the lattice SO coupling can be simulated by the laser-induced-gauge-field method and give the specific laser setting and parameters to realize the intrinsic SO coupling. Furthermore, we have established the relation between spin Chern number and spin-atomic density, so we can then detect the spin Chern number through the standard density-profile technique used in atomic systems.

ACKNOWLEDGMENTS

S. L. Zhu was supported in part by NSF of China (No. 10974059) and the State Key Program for Basic Research of China (No. 2006CB921801 and No. 2007CB925204). This work was supported by NSF of China under Grants No. 10874235, No. 10934010, and No. 60978019, and by NKBRSFC under Grants No. 2009CB930701, No. 2010CB922904, and No. 2011CB921500.

[1] M. Lewenstein, A. Sanpera, V. Ahufinger, B. Damski, A. Sen(De), and U. Sen, Adv. Phys. **56**, 243 (2007).
[2] J. Ruseckas, G. Juzeliūnas, P. Öhberg, and M. Fleischhauer, Phys. Rev. Lett. **95**, 010404 (2005).
[3] K. Osterloh, M. Baig, L. Santos, P. Zoller, and M. Lewenstein, Phys. Rev. Lett. **95**, 010403 (2005).
[4] G. Juzeliūnas, J. Ruseckas, P. Öhberg, and M. Fleischhauer, Phys. Rev. A **73**, 025602 (2006).
[5] S. L. Zhu, H. Fu, C. J. Wu, S. C. Zhang, and L. M. Duan, Phys. Rev. Lett. **97**, 240401 (2006); S. L. Zhu, D. W. Zhang, and Z. D. Wang, *ibid.* **102**, 210403 (2009).
[6] Y. J. Lin, R. L. Compton, A. R. Perry, W. D. Phillips, J. V. Porto, and I. B. Spielman, Phys. Rev. Lett. **102**, 130401 (2009).
[7] Y. J. Lin, R. L. Compton, K. Jiménez-García, J. V. Porto, and I. B. Spielman, Nature (London) **462**, 628 (2009).
[8] K. v. Klitzing, G. Dorda, and M. Pepper, Phys. Rev. Lett. **45**, 494 (1980); D. C. Tsui, H. L. Stormer, and A. C. Gossard, *ibid.* **48**, 1559 (1982); D. J. Thouless, M. Kohmoto, M. P. Nightingale, and M. den Nijs, *ibid.* **49**, 405 (1982); B. I. Halperin, Phys. Rev. B **25**, 2185 (1982); Q. Niu, D. J. Thouless, and Y. S. Wu, *ibid.* **31**, 3372 (1985); Y. Hatsugai, Phys. Rev. Lett. **71**, 3697 (1993).
[9] T. D. Stanescu, V. Galitski, J. Y. Vaishnav, C. W. Clark, and S. Das Sarma, Phys. Rev. A **79**, 053639 (2009).
[10] A. Bermudez, N. Goldman, A. Kubasiak, M. Lewenstein, and M. A. Martin-Delgado, New J. Phys. **12**, 033041 (2010).
[11] I. I. Satija, D. C. Dakin, J. Y. Vaishnav, and C. W. Clark, Phys. Rev. A **77**, 043410 (2008).
[12] L. B. Shao, S. L. Zhu, L. Sheng, D. Y. Xing, and Z. D. Wang, Phys. Rev. Lett. **101**, 246810 (2008).
[13] X. J. Liu, X. Liu, C. Wu, and J. Sinova, Phys. Rev. A **81**, 033622 (2010).
[14] N. Goldman, I. Satija, P. Nikolic, A. Bermudez, M. A. Martin-Delgado, M. Lewenstein, and I. B. Spielman, e-print arXiv:1002.0219v2; A. Bermudez, L. Mazza, M. Rizzi, N. Goldman, M. Lewenstein, and M. A. Martin-Delgado, e-print arXiv:1004.5101v1.
[15] C. N. Varney, K. Sun, M. Rigol, and V. Galitski, Phys. Rev. B **82**, 115125 (2010).
[16] T. D. Stanescu, V. Galitski, and S. D. Sarma, Phys. Rev. A **82**, 013608 (2010).
[17] F. D. M. Haldane, Phys. Rev. Lett. **61**, 2015 (1988).
[18] C. L. Kane and E. J. Mele, Phys. Rev. Lett. **95**, 146802 (2005); **95**, 226801 (2005).
[19] B. A. Bernevig, T. L. Hughes, and S. C. Zhang, Science **314**, 1757 (2006).
[20] L. Fu, C. L. Kane, and E. J. Mele, Phys. Rev. Lett. **98**, 106803 (2007).
[21] L. Fu and C. L. Kane, Phys. Rev. B **76**, 045302 (2007).
[22] J. Moore, Nature Phys. **5**, 378 (2009); Nature (London) **460**, 1090 (2009); **464**, 194 (2010).
[23] M. Büttiker, Science **325**, 278 (2009).
[24] S. Murakami, Phys. Rev. Lett. **97**, 236805 (2006).
[25] M. König, S. Wiedmann, C. Breüne, A. Roth, H. Buhmann, L. W. Molenkamp, X. L. Qi, and S. C. Zhang, Science **318**, 766 (2007).
[26] D. Hsieh, D. Qian, L. Wray, Y. Xia, Y. S. Hor, R. J. Cava, and M. Z. Hasan, Nature (London) **452**, 970 (2008); D. Hsieh *et al.*, *ibid.* **460**, 1101 (2009); Science **323**, 919 (2009); P. Roushan *et al.*, Nature (London) **460**, 1106 (2009).
[27] H. Zhang, C. X. Liu, X. L. Qi, X. Dai, Z. Fang, and S. C. Zhang, Nature Phys. **5**, 438 (2009); X. L. Qi, R. Li, J. Zang, and S. C. Zhang, Science **323**, 1184 (2009); Y. L. Chen *et al.*, *ibid.* **325**, 178 (2009).
[28] A. S. Sørensen, E. Demler, and M. D. Lukin, Phys. Rev. Lett. **94**, 086803 (2005).
[29] R. N. Palmer and D. Jaksch, Phys. Rev. Lett. **96**, 180407 (2006).
[30] R. O. Umucalilar, H. Zhai, and M. Ö. Oktel, Phys. Rev. Lett. **100**, 070402 (2008).
[31] X. J. Liu, M. F. Borunda, X. Liu, and J. Sinova, Phys. Rev. Lett. **102**, 046402 (2009); X. J. Liu, X. Liu, L. C. Kwek, and C. H. Oh, *ibid.* **98**, 026602 (2007).
[32] Y. Li, C. Bruder, and C. P. Sun, Phys. Rev. Lett. **99**, 130403 (2007).
[33] T. D. Stanescu, C. Zhang, and V. Galitski, Phys. Rev. Lett. **99**, 110403 (2007).
[34] H. M. Guo and M. Franz, Phys. Rev. B **80**, 113102 (2009).

[35] Z. Wang and P. Zhang, Phys. Rev. B **76**, 064406 (2007); **77**, 125119 (2008).
[36] D. N. Sheng, Z. Y. Weng, L. Sheng, and F. D. M. Haldane, Phys. Rev. Lett. **97**, 036808 (2006).
[37] A. Mielke, J. Phys. A **24**, L73 (1991); **24**, 3311 (1991); **25**, 4335 (1992).
[38] L. Santos, M. A. Baranov, J. I. Cirac, H. U. Everts, H. Fehrmann, and M. Lewenstein, Phys. Rev. Lett. **93**, 030601 (2004).
[39] B. Damski, H. Fehrmann, H. U. Everts, M. Baranov, L. Santos, and M. Lewenstein, Phys. Rev. A **72**, 053612 (2005).
[40] C. Lee, T. J. Alexander, and Y. S. Kivshar, Phys. Rev. Lett. **97**, 180408 (2006).
[41] N. Goldman, A. Kubasiak, A. Bermudez, P. Gaspard, M. Lewenstein, and M. A. Martin-Delgado, Phys. Rev. Lett. **103**, 035301 (2009).